An Output Power Fluctuation Suppression Method of DWPT Systems Based on Dual-receiver Coils and Voltage Doubler Rectifier

Shunpan Liu, *Student Member, IEEE,* Yong Li, *Senior Member, IEEE,* Yihao Wu, *Student Member,* Lingyun Zhou, *Student Member, IEEE,* Xing Zhao, *Member, IEEE,* Ruikun Mai, *Member, IEEE,* and Zhengyou He, *Senior Member, IEEE*

***Abstract*—In Dynamic Wireless Power Transfer (DWPT) systems, the power oscillation phenomena caused by coupling fluctuation are always hard to avoid. Moreover, if the adjacent track coils are excited by different inverters without synchronized drive signals, there will be severe power oscillations due to the frequency difference between the track coil currents. To address these issues, this work proposes a novel DWPT system based on dual-receiver coils and the Voltage Doubler (VD) rectifier. Depending on whether the induced voltages of the two receiver coils are balanced, the rectifier will switch between full-bridge mode and VD mode with no extra controller to maintain the system output under different positions. By designing the dimensions of the coupler, the DWPT system can achieve excellent output stability while avoiding the oscillation caused by the frequency difference between the track coil currents. In addition, the operation characteristic, power divisions, and boundary conditions of each operation mode are clarified. Finally, a 2.2 m 220 V-800 W prototype is built. The experimental results show that even with the track current frequency difference, the output voltage fluctuation is limited to 3.4% during motion, and the system efficiency remains above 90.76% in the case of an 8 cm air gap.**

***Index Terms*—Dynamic wireless power transfer (DWPT), Power fluctuation suppression, Dual-receiver coils, Voltage doubler rectifier.**

I. Introduction

In recent years, the applications of electric vehicles and automatic guided vehicles have developed rapidly. However, the onboard battery capacity limitation, distance anxiety, and inconvenient charging operations are still roadblocks to the mass acceptance of these vehicles. To solve these issues, the placement of electric chargers along the moving way of vehicles is necessary. Compared with the wired charger, which requires vehicles to park at a fixed position and affects the operational efficiency of the vehicles during the charging process, Dynamic Wireless Power Transfer (DWPT) technology is an attractive choice nowadays [1]-[5]. With the track coils embedded in the road and the receiver coils set under the bottom of the vehicles, the DWPT system can conveniently charge the vehicles in the moving process.

Nowadays, according to the length of the track coils, the DWPT system can be divided into two categories. The first is the long-track type [6]-[9], which is always designed to be tens or hundreds of meters. Although it can provide a flat magnetic field for vehicles, the Electromagnetic Interference (EMI) and power loss of the track coils are difficult to limit [10]-[12]. The second is the short-segment type [13], [14]. By setting multiple short track coils and individually controlling them, the segmented track coils can be excited one by one when vehicles move along the track. The length of these coils is equal to or just several times longer than the receiver coils. Thus, only one or two track coils will be excited simultaneously, optimizing the EMI and reducing coil loss. However, the electromagnetic field generated by the segmented track coils is not flat enough, which results in power null and pulsation phenomena [11], [15]. Although the closed-loop controlled converter can assist in regulating the system output [16]-[19], the power fluctuations are still hard to avoid, while the frequent regulating of the converters will bring severe burdens on the controller and undesired power loss to the converter.

To eliminate the power null and pulsation phenomena caused by the variation of the mutual inductances between track coils and receiver coils, adjusting the width of the track coils is an available method [15], [20], [21]. However, there is always unavoidable cross-coupling between the adjacent track coils, negatively affecting the system gain and efficiency. To solve this issue, some researchers adopted the Double-D Quadrature (DDQ) structure [11] to ensure that the track coils can be arranged snugly with a relatively flat electromagnetic field. Moreover, several researchers report some methods of setting dual [22]-[24] or multiple [25] receiver coils to mitigate the power fluctuation issue. However, the power fluctuation is still hard to eliminate completely, especially when the receiver moves above the adjacent parts of the track coils.

In addition, in long-distance DWPT systems with multiple track coils, a single inverter can only excite one or several adjacent track coils. If there is a tiny frequency difference between the currents in the adjacent track coils due to the lack of synchronization of the inverters, when the vehicle moves

Manuscript received June 15, 2022; revised August 31, and September 24, 2022; accepted October 06, 2022.This work was supported in part by the funding of the National Natural Science Foundation of China under Grant 51907169, in part by the Sichuan Science and Technology Innovation Program under Grant 2022JDRC0078, and in part by the Original Scientific Research Equipment Training Project in Southwest Jiaotong University. (*Corresponding author: Yong Li*)

S. Liu, Y. Li, L Zhou, R. Mai and Z. He are with the Key Laboratory of Magnetic Suspension Technology and Maglev Vehicle, Ministry of Education, Southwest Jiaotong University, and the School of Electrical Engineering, Southwest Jiaotong University, Chengdu 610031, China (e-mail: liusp@my.swjtu.edu.cn, leeo1864@163.com, zhouly@my.swjtu.edu.cn, mairk@swjtu.edu.cn, hezy@home.swjtu.edu.cn.).

Yihao Wu is with the Department of Electrical and Computer Engineering, University of Texas at Austin, Austin, TX 78712, USA. (e-mail: yw25243@utexas.edu.)

X. Zhao is with the School of Physics, Engineering and Technology with University of York, York YO10 5DD, U.K. (e-mail: xing.zhao@york.ac.uk.)

above the adjacent parts of the track coils, the voltages induced from different track coils contain huge harmonics and distortions. This issue always exists and is hard to avoid because of the manufacturing tolerance of the crystals in different Microprogrammed Control Units (MCUs). Generally, the current frequency difference between the adjacent track coils can reach about 5‰. For example, if the current frequency in one track coil is defined as *f*, that in the other track coil might reach (1+5‰)·*f*. However, such a tiny frequency difference will also cause severe power oscillation.

To achieve high-frequency current synchronization in different inverters, a few researchers have proposed some signal synchronization methods for inverters based on Master-Slave (MS) segmented driving technology [10]. By detecting the receiver's position, the MS controller will provide the drive signal to the corresponding master inverter and its adjacent slaver inverter. Nevertheless, in practice, the distance between the placement positions of the different inverters can be pretty long. Meanwhile, with the complex surrounding electromagnetic environment, the drive signals will be delayed, interfered with, and even interrupted by the unavoidable EMI. Nowadays, this issue still lacks available solutions.

In DWPT applications, most of the electrical device is connected to the output DC bus of the DWPT system, e.g., energy storage devices, traction loads, and lighting devices. Thus, achieving a Constant Voltage (CV) output for the DC bus is vital and necessary [26], [27]. In this paper, a novel receiver structure and topology are proposed to achieve a CV output and avoid the power oscillation caused by the current frequency difference between two adjacent track coils in the DWPT system. The main contributions and works are introduced as follows.

The VD-rectifier-based dual-receiver DWPT system is proposed to maintain CV output when the vehicle moves along the track. When the induced voltages of the receiver coils are balanced, the rectifier can be regarded as a full-bridge (FB) rectifier with two series-connected receiver coils transferring power cooperatively. When the induced voltages are not balanced, only the receiver coil with a higher induced voltage can output power with a doubled output voltage, and the current in the other coil will be cut-off. As a result, when the receiver moves above the adjacent part of the track coils, only the receiver coil with higher induced voltage can transfer power from only one track coil, and power oscillations caused by the current frequency difference can be theoretically avoided.

Meanwhile, based on the operating situation of the rectifier and receiver coils, three operation modes of the receiver are classified. By clarifying the characteristic of each mode, the accurate mathematical models of power divisions, loop currents, and boundary conditions of the proposed system are established. Moreover, based on the system model and essential factors analysis of the power oscillation caused by the current frequency difference, the magnetic coupler of the proposed system is designed with precise principles and goals to practically achieve dynamic CV characteristics.

Finally, a 2.2 m 220 V-800 W prototype is built to verify the dynamic output characteristic of the proposed DWPT system. The experimental results show that even with the track current frequency difference, the output voltage fluctuation is limited to 3.4% during motion, and the system efficiency remains above 90.7%.

II. Analysis of the Single Receiver DWPT System

To clarify the power fluctuation issue, this section introduces a typical single receiver DWPT system firstly as follows.

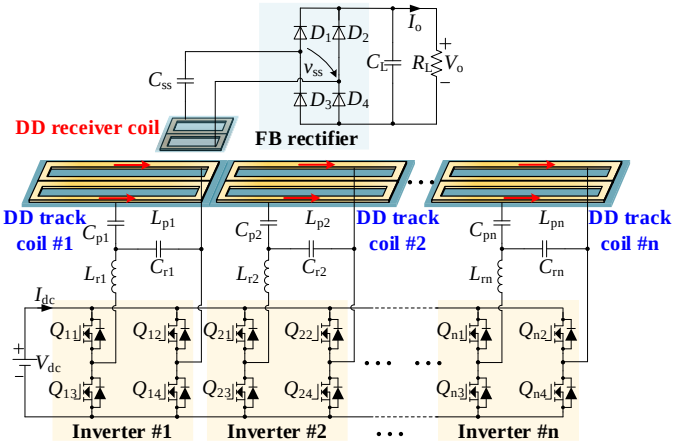

Fig. 1. The generic view of the single receiver DWPT system.

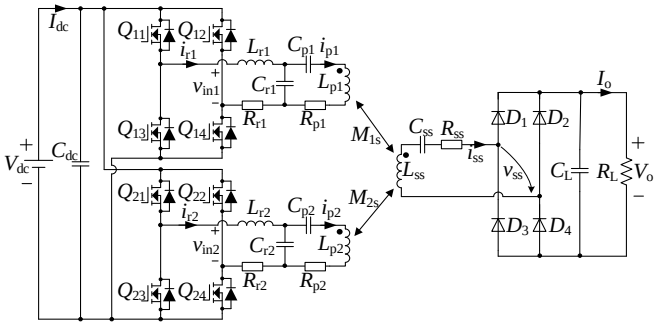

Fig. 2. The equivalent circuit of the single receiver DWPT system.

A. Description of the Single Receiver System

Fig. 1 shows a generic view of the conventional single receiver DWPT system. On the ground side, *n* FB inverters (Q_{i1}-Q_{i4}, 1≤i≤n) are parallel-connected with the same DC power source V_{dc}, and each inverter connects an Inductor-Capacitor-Capacitor (LCC) compensation network (L_{ri}, C_{ri}, and C_{pi}). Meanwhile, segmented DD track coils (L_{pi}) are arranged straight. On the vehicle side, DD receiver coil L_{ss} is set to pick up energy. C_{ss} is the compensated capacitor of the receiver coil. Diodes D_1-D_4 form the FB rectifier. V_o and I_o are the DC voltage and current on the load resistance R_L.

Generally, when the vehicle moves along the track coils, the receiver coil will be coupled with two track coils at most. Thus, we can have a simplified system equivalent circuit, as shown in Fig. 2. Here, track coils #1 and #2 with their corresponding inverters and compensation networks are analyzed as an example. M_{1s} and M_{2s} are mutual inductances between the track and receiver coils. R_{r1}, R_{r2}, R_{p1}, R_{p2}, and R_{ss}, are the equivalent series resistances (ESRs) of each loop. v_{in1} and v_{in2} are the AC voltage of inverters #1 and #2, while v_{ss} is the AC voltage of the rectifier. It is worth noting that, the distances between the track coils and between the receiver coils should be large enough so that the cross-coupling between the coils on the same side can be neglected. Then, ignoring the ESRs, Kirchhoff's voltage equations are established as

$$\begin{cases} \dot{V}_{\text{in1(1)}} = \left(j\omega L_{\text{r1}} + 1/j\omega C_{\text{r1}}\right)\cdot \dot{I}_{\text{r1}} - 1/j\omega C_{\text{r1}}\cdot \dot{I}_{\text{p1}} \\ \dot{V}_{\text{in2(1)}} = \left(j\omega L_{\text{r2}} + 1/j\omega C_{\text{r2}}\right)\cdot \dot{I}_{\text{r1}} - 1/j\omega C_{\text{r2}}\cdot \dot{I}_{\text{p2}} \\ j\omega M_{\text{1s}}\dot{I}_{\text{ss}} - 1/j\omega C_{\text{r1}}\cdot \dot{I}_{\text{r1}} + \left(j\omega L_{\text{p1}} + 1/j\omega C_{\text{r1}} + 1/j\omega C_{\text{p1}}\right)\dot{I}_{\text{p1}} = 0 \\ j\omega M_{\text{2s}}\dot{I}_{\text{ss}} - 1/j\omega C_{\text{r2}}\cdot \dot{I}_{\text{r2}} + \left(j\omega L_{\text{p2}} + 1/j\omega C_{\text{r2}} + 1/j\omega C_{\text{p2}}\right)\dot{I}_{\text{p2}} = 0 \\ j\omega M_{\text{1s}}\dot{I}_{\text{p1}} + j\omega M_{\text{2s}}\dot{I}_{\text{p2}} - \left(j\omega L_{\text{ss}} + 1/j\omega C_{\text{ss}}\right)\cdot \dot{I}_{\text{ss}} = \dot{V}_{\text{ss(1)}} \end{cases} . \quad (1)$$

When the compensation networks are resonant, we have

$$\begin{cases} j\omega L_{\text{r1}} + 1/j\omega C_{\text{r1}} = 0 & j\omega L_{\text{p1}} + 1/j\omega C_{\text{r1}} + 1/j\omega C_{\text{p1}} = 0 \\ j\omega L_{\text{r2}} + 1/j\omega C_{\text{r2}} = 0 & j\omega L_{\text{p2}} + 1/j\omega C_{\text{r2}} + 1/j\omega C_{\text{p2}} = 0 \\ j\omega L_{\text{ss}} + 1/j\omega C_{\text{ss}} = 0 \end{cases}, \quad (2)$$

where ω is the system angular frequency, $v_{\text{in1(1)}}$, $v_{\text{in2(1)}}$, and $v_{\text{ss(1)}}$ are the fundamental component of v_{in1}, v_{in2}, and v_{ss}. Substituting (2) into (1), the rectifier input voltage can be solved as

$$\dot{V}_{\text{ss(1)}} = M_{\text{1s}}\dot{V}_{\text{in1(1)}}/L_{\text{r1}} + M_{\text{2s}}\dot{V}_{\text{in2(1)}}/L_{\text{r2}} . \quad (3)$$

With the FB diode rectifier, the relationship between the voltage and current of the AC and DC side of the diode rectifier can be expressed as

$$\begin{cases} V_{\text{o}} = \pi V_{\text{ss(1)}}/2\sqrt{2} \\ I_{\text{o}} = 2\sqrt{2} I_{\text{ss}}/\pi \end{cases}, \quad (4)$$

where $V_{\text{ss(1)}}$ is the Root-Mean-Square (RMS) value of the $v_{\text{ss(1)}}$, and I_{ss} is the RMS value of the receiver coil current i_{ss}.

B. Magnetic Coupler of the Single Receiver System

This section introduces two segmented track coils to simplify the system analysis. The segmented magnetic coupler of the single receiver DWPT system is shown in Fig. 3, and the basic dimensions are listed in TABLE I. The finite-element-method model is built in ANSYS MAXWELL software to assist the coupler design, and the simulated results are plotted in Fig. 4.

To eliminate the cross-coupling between the track coils and avoid circulation currents in both inverters and track coils, the distance between track coils d_{tt} is set as 100 mm. Therefore, the mutual inductance between the track coils can be kept below 0.5 uH, which can be regarded as decoupled. However, the cost of increasing d_{tt} is the coupling fall area in the adjacent part of the track coils, as shown in Fig. 4. In this area, the sum of M_{1s} and M_{2s} is lower than 20% of the rated value, which easily triggers the low-voltage protection of the onboard load equipment.

C. Dynamic Performance

To clear the dynamic performance of the single-receiver DWPT system, we input the simulated mutual inductance results into Simulink software. With the circuit parameters listed in TABLE II, the simulated waveforms are shown in Fig. 5.

Here, the frequency of i_{p1} is always set as f, and the frequency of i_{p2} is set as f, (1+2‰)·f, and (1+5‰)·f, in turn, to verify the system output characteristic with a tiny frequency difference between adjacent coils. Meanwhile, R_{L} is set to 60.5 Ω, and the system output power is 800 W. In Fig. 5(a), it is obvious that the single receiver system can provide a constant output when the receiver moves above the middle range of the track coils. However, when the vehicle is above the adjacent area between the track coils, V_{o} will sharply drop by over 20%. Moreover, as shown in Fig. 5(b) and (c), the tiny difference in the adjacent coil current frequency will not only aggravate the fluctuation of the system output voltage V_{o}, but also result in the oscillation in the receiver coil current, which further leads to a more severe transfer power oscillation and damage to the onboard devices. The oscillation frequency f_{r} is the difference between current frequencies of the two track coils. When the frequency of i_{p2} is (1+2‰)·f, the oscillation frequency f_{r}=2‰·f, and the overcurrent of i_{ss} is more than five times compared to the rated value. Similarly, when the frequency of i_{p2} is (1+5‰)·f, f_{r} is increased to 5‰·f, and the overcurrent of i_{ss} is near to four times of the rated value.

TABLE I THE KEY PARAMETERS OF THE SEGMENTED MAGNETIC COUPLER

Symb.	*Para.*	*Val.*
l_{tc}	Length of the track coils	1000 mm
l_{tf}	Length of the track coils' ferrite	2400 mm
w_{tc}	Width of the track coils	400 mm
w_{tf}	Width of the track coils' ferrite	500 mm
d_{tc}	Line width of the track coils	20 mm
d_{tt}	Distance between two track coils	100 mm
l_{rc}	Length of the receiver coils	250 mm
l_{rf}	Length of the receiver coils' ferrite	300 mm
w_{rc}	Width of the receiver coils	400 mm
w_{rf}	Width of the receiver coils' ferrite	500 mm
d_{rc}	Line width of the receiver coils	33 mm
g	Air gap	80 mm

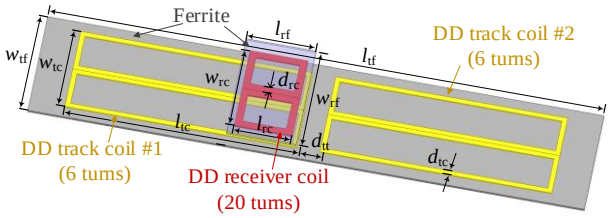

Fig. 3. The magnetic coupler in the single receiver DWPT system.

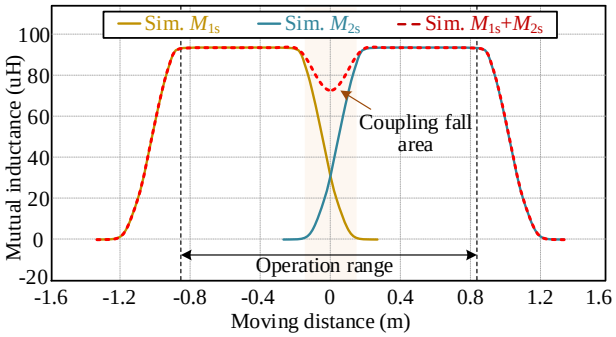

Fig. 4. Mutual inductances of the single receiver DWPT system.

TABLE II SYSTEM SPECIFICATION AND PARAMETER VALUES

Sym.	*Val.*	*Sym.*	*Val.*	*Sym.*	*Val.*	*Sym.*	*Val.*
V_{dc}	240 V	V_{o}	220 V	I_{o}	3.6 A	f	85 kHz
L_{r1}	92 uH	L_{r2}	92 uH	L_{p1}	274 uH	L_{p2}	274 uH
C_{r1}	38.1 nF	C_{r2}	38.1 nF	C_{p1}	19.3 nF	C_{p2}	19.3 nF
R_{r1}	0.11 Ω	R_{r1}	0.11 Ω	R_{p1}	0.31 Ω	R_{p2}	0.31 Ω
L_{ss}	732 uH	C_{ss}	4.8 nF	R_{ss}	0.83 Ω		

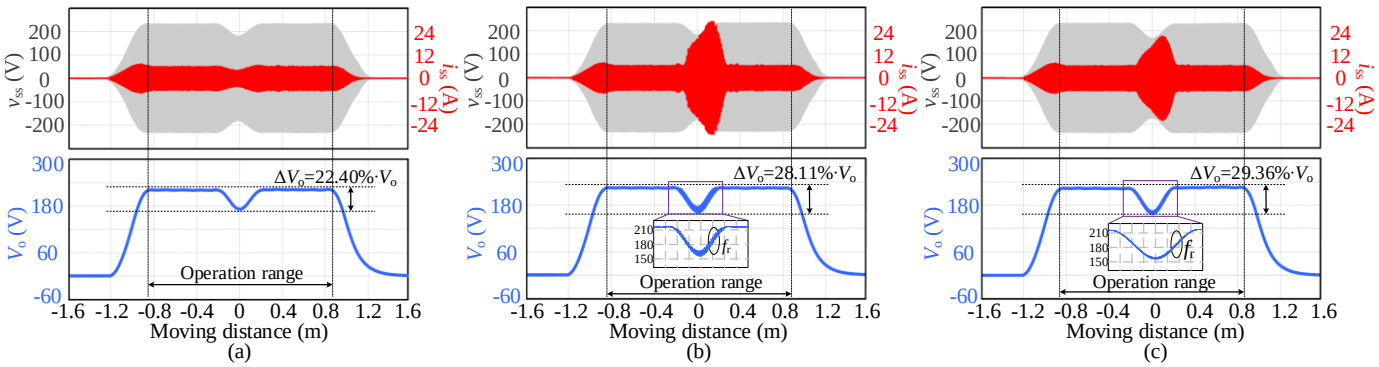

Fig. 5 The dynamic waveforms of the induced voltages and currents of receiver coils, system output voltage of the conventional single receiver system when the current frequency of i_{p1} is f and the current frequency of i_{p2} is (a) f, (b) (1+2‰)·f, and (c) (1+5‰)·f.

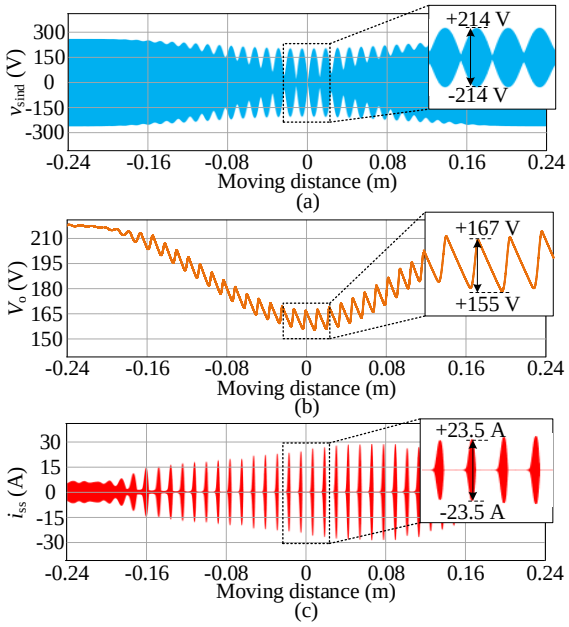

Fig. 6 Simulated waveforms of (a) v_{sind}, (b) V_o, and (c) i_{ss} with $\Delta\omega$=2‰ when the receiver moves above the adjacent area of the track coils.

D. Analysis of the power oscillation

It is not difficult to deduce that the root cause of the system power oscillation when the receiver moves above the adjacent area of the track coils is the frequency difference in the induced voltage of the receiver coil from different track coils. Here, the time domain expression of the induced voltage of the receiver coil v_{sind} can be defined as

$$v_{sind}(t) = M_{1s} v_{in1(1)}(t)/L_{r1} + M_{2s} v_{in2(1)}(t)/L_{r2}\,, \tag{5}$$

where $v_{in1(1)}(t) = \dfrac{4V_{dc}\sin(\omega t)}{\pi}$ and $v_{in2(1)}(t) = \dfrac{4V_{dc}\sin((\omega+\Delta\omega)t)}{\pi}$ are the fundamental components of the inverter output voltages. $\Delta\omega$ is the angular frequency difference between the two adjacent inverters. Thus, based on the wave superposition analysis method, v_{sind} can be further derived as

$$\begin{aligned} v_{sind}(t) &= 4V_{dc}\left[M_{1s}\sin(\omega t)/L_{r1} + M_{2s}\sin((\omega+\Delta\omega)t)/L_{r2}\right]/\pi \\ &= \frac{4}{\pi}V_{dc}\sqrt{\left(\frac{M_{1s}}{L_{r1}}\right)^2 + \left(\frac{M_{2s}}{L_{r2}}\right)^2 + 2\cdot\frac{M_{1s}}{L_{r1}}\cdot\frac{M_{2s}}{L_{r2}}\cdot\cos(\Delta\omega\cdot t)}\cdot\sin(\omega t+\theta) \end{aligned}\,, \tag{6}$$

where $\theta = \arcsin\left(\dfrac{M_{2s}\sin(\Delta\omega\cdot t)/L_{r2}}{\sqrt{\left(\frac{M_{1s}}{L_{r1}}\right)^2 + \left(\frac{M_{2s}}{L_{r2}}\right)^2 + \frac{2M_{1s}M_{2s}}{L_{r1}L_{r2}}\cos(\Delta\omega\cdot t)}}\right)$

According to (6), we can draw two conclusions as follows:

1) Since there is a tiny difference between the voltages induced from the two different track coils, the amplitude of v_{sind} will also oscillate with the frequency $\Delta\omega$. Meanwhile, the angular frequency of the induced voltage itself will also be affected. With the variations on the relationship between the amplitudes of $v_{in1(1)}$ and $v_{in2(1)}$, the angular frequency of v_{sind} will vary within ω to $\omega+\Delta\omega$.

2) If $\Delta\omega\neq0$, the amplitude of v_{sind} will oscillate from $4V_{dc}|M_{1s}/L_{r1}-M_{2s}/L_{r2}|/\pi$ to $4V_{dc}|M_{1s}/L_{r1}+M_{2s}/L_{r2}|/\pi$. Actually, the inductance of L_{r1} and L_{r2} are approximately equal, and when the receiver moves above the central position of the adjacent part of the track coils, M_{1s} and M_{2s} can be also regarded as equal. Thus, in the whole moving process, the envelope of v_{sind} will cover the range from 0 to the maximum value of $4V_{dc}|M_{1s}/L_{r1}+M_{2s}/L_{r2}|/\pi$.

When the receiver moves above the adjacent part of two track coils, the detail waveforms of v_{sind}, V_o, and i_{ss} under $\Delta\omega$=2‰ are shown in Fig. 6 to analyze the power oscillation issue as an example. It is obvious that there are apparent oscillations on the induced voltage v_{sind}, which also cause the ripple on the system DC output voltage V_o, as shown in Fig. 6 (a) and (b). Moreover, the power oscillation is reflected in the current oscillation of the receiver coil. Due to the clamping effect of the diode rectifier, only when the RMS value of the induced voltage V_{sind} is higher than $2\sqrt{2}\cdot V_o/\pi$, the rectifier will output power, i.e., the RMS value of the receiver coil current $I_{ss} > 0$. Thus, the current i_{ss} tends to be of the short pulse in Fig. 6(c).

It should be noted that the peak value of the pulse current i_{ss} is determined by the difference between $V_{sind}(t)$ and $2\sqrt{2}\cdot V_o(t)/\pi$, and the length of the time period that $V_{sind}(t)$ is higher than $2\sqrt{2}\cdot V_o(t)/\pi$, which is always negatively correlated with $\Delta\omega$. Meanwhile, the dynamic characteristic of the receiver circuit will also affect the overcurrent in the receiver coil. Generally, the current impulse of i_{ss} is always much higher than the rated value of i_{ss}.

In conclusion, the induced voltage is the sum of the induced voltage from two different track coils in the single-receiver system. Thus, when there is a tiny current frequency difference between the adjacent track coils due to the failure of syn-

chronization of the inverters, the power oscillation is hard to be avoided in the process that the receiver moves above the adjacent area of the track coils. To solve this issue, an available method to avoid the receiver transferring power from two different track coils is required.

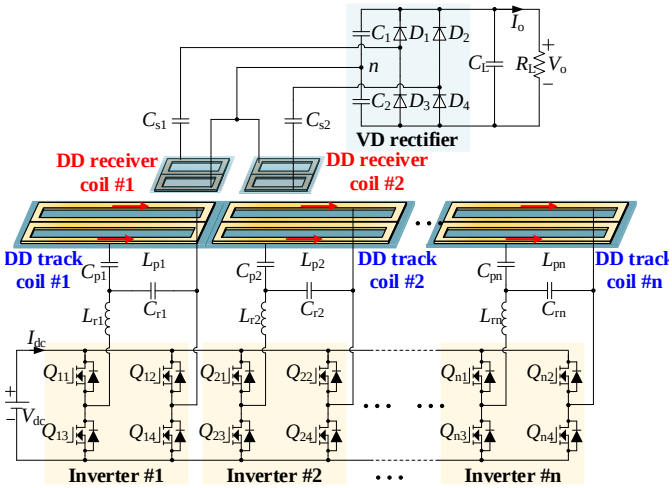

Fig. 7. The generic view of the proposed dual-receiver DWPT system.

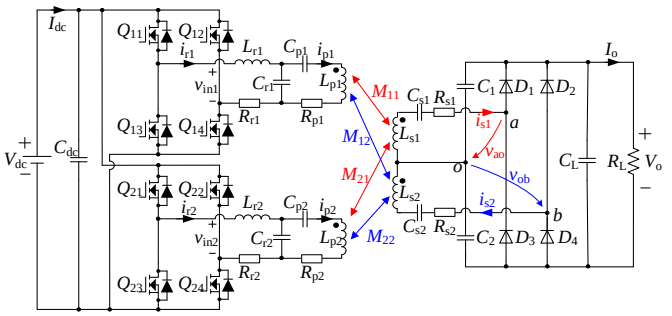

Fig. 8. The equivalent circuit of the proposed DWPT system.

III. Analysis of the Dual-Receiver DWPT System

A. Circuit Description and Analysis

In this paper, a novel DWPT system based on dual-receiver coils and a VD rectifier is proposed. Fig. 7 shows a generic view of the proposed system. The main difference between the proposed system and the conventional single-receiver system is the topology on the receiver side. Here, two identical DD receiver coils L_{s1} and L_{s2} are set with their series compensated capacitors C_{s1} and C_{s2}. Both receiver coils are connected to the VD rectifier consisting of two capacitors (C_1, C_2) and four diodes (D_1-D_4). Similarly, the distance between the receiver coils is large enough to eliminate the cross-coupling.

The simplified equivalent circuit of the proposed DWPT system is depicted in Fig. 8. v_{ao} and v_{ob} are the AC input voltages of the VD rectifier, i_{s1} and i_{s2} are the coil currents in the receiver coils. M_{11}, M_{12}, M_{21}, and M_{22} are mutual inductances between the track and receiver coils. R_{s1} and R_{s2} are the ESRs of the receiver coils. Then, ignoring ESRs, the Kirchhoff's equations of the proposed DWPT system can be established as

$$\begin{cases} \dot{V}_{in1(1)} = \left(j\omega L_{r1} + 1/j\omega C_{r1}\right)\cdot \dot{I}_{r1} - 1/j\omega C_{r1}\cdot \dot{I}_{p1} \\ \dot{V}_{in2(1)} = \left(j\omega L_{r2} + 1/j\omega C_{r2}\right)\cdot \dot{I}_{r1} - 1/j\omega C_{r2}\cdot \dot{I}_{p2} \\ j\omega M_{11}\dot{I}_{s1} + j\omega M_{12}\dot{I}_{s2} - 1/j\omega C_{r1}\cdot \dot{I}_{r1} + \left(j\omega L_{p1} + 1/j\omega C_{r1} + 1/j\omega C_{p1}\right)\dot{I}_{p1} = 0 \\ j\omega M_{21}\dot{I}_{s1} + j\omega M_{22}\dot{I}_{s2} - 1/j\omega C_{r2}\cdot \dot{I}_{r2} + \left(j\omega L_{p2} + 1/j\omega C_{r2} + 1/j\omega C_{p2}\right)\dot{I}_{p2} = 0 \\ j\omega M_{11}\dot{I}_{p1} + j\omega M_{21}\dot{I}_{p2} - \left(j\omega L_{s1} + 1/j\omega C_{s1}\right)\cdot \dot{I}_{s1} = \dot{V}_{ao(1)} \\ j\omega M_{12}\dot{I}_{p1} + j\omega M_{22}\dot{I}_{p2} - \left(j\omega L_{s2} + 1/j\omega C_{s2}\right)\cdot \dot{I}_{s2} = \dot{V}_{ob(1)} \end{cases}, \quad (7)$$

where $v_{ao(1)}$ and $v_{ob(1)}$ are the fundamental components of v_{ao} and v_{ob}. When the compensation networks are completely resonant, $\dot{V}_{ao(1)}$ and $\dot{V}_{ob(1)}$ can be solved as

$$\begin{cases} \dot{V}_{ao(1)} = M_{11}\dot{V}_{in1(1)}/L_{r1} + M_{21}\dot{V}_{in2(1)}/L_{r2} \\ \dot{V}_{ob(1)} = M_{12}\dot{V}_{in1(1)}/L_{r1} + M_{22}\dot{V}_{in2(1)}/L_{r2} \end{cases}. \quad (8)$$

B. Characteristics of the Dual-receiver DWPT System

In the proposed DWPT system, when the vehicle moves to different positions, the variations of the mutual inductances between the track coils and the receiver coils will switch the receiver into different operation modes. Here, the characteristics of these operation modes are analyzed as follows.

1) Mode A: FB rectifier mode

If the RMS value and the frequency of the rectifier input voltage V_{ao} and V_{ob} are identical, the receiver can be regarded as series-connected dual receiver coils with the diode rectifier, and the rectifier will operate in the FB mode, and the currents flow to C_1 and C_2 are quite small, as shown in Fig. 9(a). The induced voltages v_{s1} and v_{s2} can be expressed as

$$\begin{cases} \dot{V}_{s1} = M_{11}\dot{V}_{in1(1)}/L_{r1} + M_{21}\dot{V}_{in2(1)}/L_{r2} = \dot{V}_{ao(1)} + \dot{I}_{s1}R_{s1} \\ \dot{V}_{s2} = M_{12}\dot{V}_{in1(1)}/L_{r1} + M_{22}\dot{V}_{in2(1)}/L_{r2} = \dot{V}_{ob(1)} + \dot{I}_{s2}R_{s2} \end{cases}. \quad (9)$$

Considering the ESRs and the forward voltage of the diodes V_F, the system output voltage V_o can be obtained as

$$V_o = \pi\left[V_{s1} + V_{s2} - I_{s1}\left(R_{s1} + R_{s2}\right)\right]/2\sqrt{2} - 2V_F, \quad (10)$$

where V_{s1} and V_{s2} are the RMS value of the induced voltages v_{s1} and v_{s2}. I_{s1} is the RMS value of current in receiver coil#1, which is equal to that in receiver coil #2 I_{s2}. The key waveforms of this mode are shown in Fig. 9(b). With the diode rectifier, the system output current I_o expressed as

$$I_o = 2\sqrt{2}I_{s1}/\pi = 2\sqrt{2}I_{s2}/\pi = V_o/R_L. \quad (11)$$

Combining (10) and (11), the exact expression of the system output voltage V_o and the coil current can be solved as

$$V_o = R_L\cdot\left(V_{s1} + V_{s2} - 4\sqrt{2}V_F/\pi\right)/\left(R_{s1} + R_{s2} + 2\sqrt{2}R_L/\pi\right). \quad (12)$$

$$I_{s1} = \left(\pi\left(V_{s1} + V_{s2}\right)/2\sqrt{2} - 2V_F\right)/\left(R_{s1} + R_{s2} + 2\sqrt{2}R_L/\pi\right). \quad (13)$$

According to (12), we know that V_o is determined by the sum of the induced voltages of the two receiver coils. Thus, to achieve the same rated output voltage as the single receiver system, the turns of each receiver coil should be halved.

2) Mode B: VD rectifier with dual coil receiving power

Continuous moving of the receiver will unavoidably cause the imbalance between V_{s1} and V_{s2}. In this situation, the rectifier will turn into VD rectifier mode, and the output power of each receiver coil is also unbalanced. If $\pi V_{s1}/\sqrt{2} - 2V_F > V_o$ and $\pi V_{s2}/\sqrt{2} - 2V_F > V_o$ are satisfied, which means the difference

between V_{s1} and V_{s2} is limited, the receiver will operate in VD rectifier mode with dual-coil receiving power. As shown in Fig. 9(c), D_1, D_3, C_1, and C_2 form the VD rectifier for receiver coil #1, while D_2, D_4, C_1, and C_2 form the other VD rectifier for receiver coil #2. Although these two VD rectifiers share the same pair of capacitors, they can still be regarded as connected in parallel. Thus, the output currents of these VD rectifiers are both input to the load, and I_o and V_o should be

$$I_o = \sqrt{2}\left(I_{s1} + I_{s2}\right)/\pi \,. \tag{14}$$

$$V_o = \sqrt{2}\left(I_{s1} + I_{s2}\right)R_L/\pi \,. \tag{15}$$

Meanwhile, the RMS values of I_{s1} and I_{s2}, which indicate the transfer power of the receiver coils, are determined as

$$\begin{cases} I_{s1} = \left[V_{s1} - \sqrt{2}\left(V_o + 2V_F\right)/\pi\right]/R_{s1} \\ I_{s2} = \left[V_{s2} - \sqrt{2}\left(V_o + 2V_F\right)/\pi\right]/R_{s2} \end{cases} . \tag{16}$$

Thus, the system output voltage V_o can be expressed as

$$V_o = \pi\left(V_{s1} - I_{s1}R_{s1}\right)/\sqrt{2} - 2V_F = \pi\left(V_{s2} - I_{s2}R_{s2}\right)/\sqrt{2} - 2V_F \,. \tag{17}$$

Although V_{ao} and V_{ob} are just half of the rectifier input voltage V_{ab} in mode A, V_o in mode B is approximately the same as that in Mode A due to the doubled voltage gain of the VD rectifier. Taking V_{s1}-$I_{s1}R_{s1}$>V_{s2}-$I_{s2}R_{s2}$ as an example, combining (15)-(17), V_o, I_{s1}, and I_{s2} can be accurately solved as

$$V_o = \frac{R_L\left(\sqrt{2}\pi\cdot\left(R_{s1}V_{s2} + R_{s2}V_{s1}\right) - 4\cdot\left(R_{s1} + R_{s2}\right)\cdot V_F\right)}{2\cdot\left(R_{s1} + R_{s2}\right)\cdot R_L + \pi^2 R_{s1}R_{s2}} \,. \tag{18}$$

$$I_{s1} = \frac{2\left(V_{s1} - V_{s2}\right)R_L + R_{s2}\left(\pi^2 V_{s1} - 2\sqrt{2}\pi V_F\right)}{2\cdot\left(R_{s1} + R_{s2}\right)\cdot R_L + \pi^2 R_{s1}R_{s2}} \,. \tag{19}$$

$$I_{s2} = \frac{2\left(V_{s2} - V_{s1}\right)R_L + R_{s1}\left(\pi^2 V_{s2} - 2\sqrt{2}\pi V_F\right)}{2\cdot\left(R_{s1} + R_{s2}\right)\cdot R_L + \pi^2 R_{s1}R_{s2}} \,. \tag{20}$$

In this situation, the transfer power of receiver coil #1 is higher than that of receiver coil #2, and the key waveforms are shown in Fig. 9(d). It is worth noting that, since R_{s1} and R_{s2} are relatively small compared with R_L, though the difference between V_{s1} and V_{s2} is limited, the difference between I_{s1} and I_{s2} is significant. According to (12) and (18), while ignoring the ESRs and V_F, V_o in Mode A and B can be regarded as the same. Meanwhile, since the two receiver coils and their VD rectifier are symmetric, when V_{s1}-$I_{s1}R_{s1}$<V_{s2}-$I_{s2}R_{s2}$, the expressions of V_o, I_{s1}, and I_{s2} are symmetric to (18)-(20). Due to space limitations, these expressions are no longer given.

3) Mode C: VD rectifier with single coil receiving power

In Fig. 9(e) and (f), when the difference between V_{s1} and V_{s2} is significant, i.e., $\pi V_{s1}/\sqrt{2} - 2V_F > V_o$ or $\pi V_{s2}/\sqrt{2} - 2V_F > V_o$ cannot be satisfied, due to the clamping effect of the VD rectifier, the receiver coil with lower induced voltage will be cut-off, and only the receiver coil with higher induced voltage can output power with the doubled output voltage. To simplify the analysis, the situation in which receiver coil #1 transfers power individually is analyzed as an example. Here we have

$$I_o = V_o/R_L = \sqrt{2}I_{s1}/\pi \,, \tag{21}$$

$$V_o = \pi\left(V_{s1} - I_{s1}R_{s1}\right)/\sqrt{2} - 2V_F \,. \tag{22}$$

Combining (21) and (22), the precise expressions of I_{s1} and V_o can be accurately solved as

$$I_{s1} = \left(\pi^2 V_{s1} - 2\sqrt{2}\pi V_F\right)/\left(2R_L + \pi^2 R_{s1}\right) , \tag{23}$$

$$V_o = R_L\cdot\left(\sqrt{2}\pi V_{s1} - 4V_F\right)/\left(2R_L + \pi^2 R_{s1}\right) . \tag{24}$$

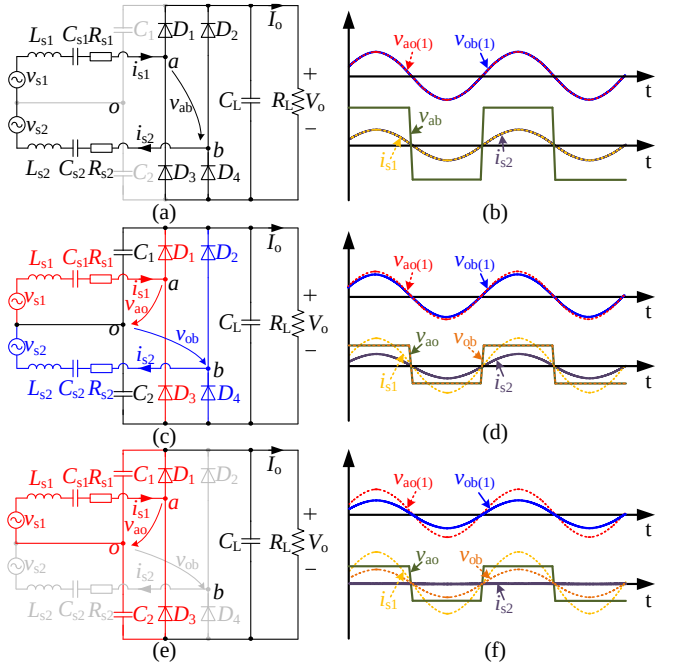

Fig. 9. Diagrams and waveforms of the receiver in Mode A, B, and C.

According to (24), although V_{s1} is only half of V_{s1}+V_{s2} in Mode A and B, with the doubled DC output voltage, V_o in this mode can still be regarded the same as in Mode A and B, which provides a foundation for power fluctuation suppression.

In conclusion, the proposed system can maintain a CV output by switching the operation modes without any extra controllers within different induced voltages of these two receiver coils. To exploit the properties of the proposed system, its magnetic coupler is designed and introduced in Section III. C.

C. Design of Magnetic Coupler of the DWPT System

To verify the performance of the proposed DWPT system, the dimension parameters of the magnetic coupler are the same as the conventional single receiver DWPT system listed in TABLE I. The only difference is that two identical DD receiver coils are set at the vehicle side. Meanwhile, the number of individual receiver coil turns is half that of the receiver coil in Section II.B. The segmented magnetic coupler of the proposed DWPT system is shown in Fig. 10. Here, two main principles should be noticed when designing the distance between the receiver coils. Firstly, the distance between the receiver coil d_{rr} should match the size and distance between the track coils d_{tt} to suppress the system power fluctuation during the moving process. Secondly, the receiver coils should be decoupled, and the overall receiver size should be limited.

Thus, the distance between receiver coils d_{rr} is set to 150 mm as an example to ensure that no matter where the receiver locates, at least one receiver coil is strongly coupled with the track coils. Due to the characteristic of the proposed DWPT system, no matter which receiver coil couples to any track coil strongly, the coupling drop area can be avoided. Meanwhile,

when d_{rr} = 150 mm, the mutual inductance between the receiver coils is lower than 0.1 uH, which means that the receiver coils are decoupled. With the assistance of ANSYS MAXWELL software, the simulated mutual inductances between the track coils and receiver coils are plotted in Fig. 12. Then, the division of the three operation modes in the proposed DWPT system can be cleared and analyzed as follow:

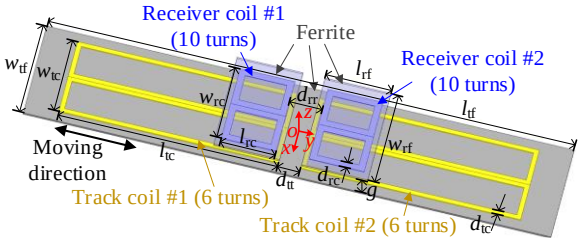

Fig. 10 The structure of the proposed segmented magnetic coupler.

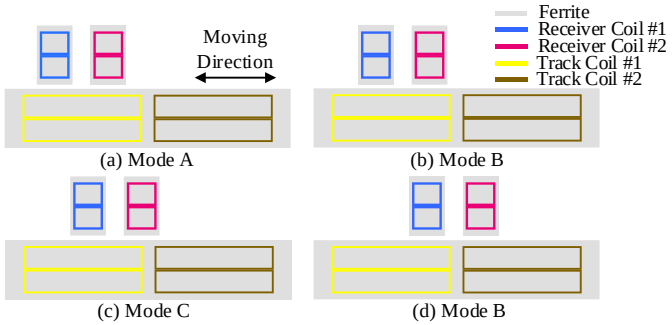

Fig. 11. The diagram of the receiver positions when the receiver operates in (a) Mode A, (b) Mode B, (c) Mode C, and (d) Mode B when the receiver moves above the adjacent part of the track coils.

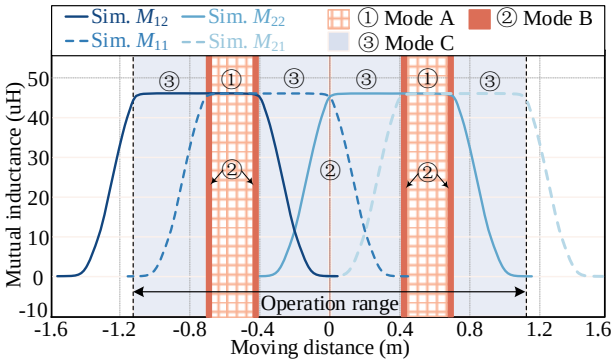

Fig. 12. Mutual inductances between track coils and receiver coils and the divisions of three operation modes.

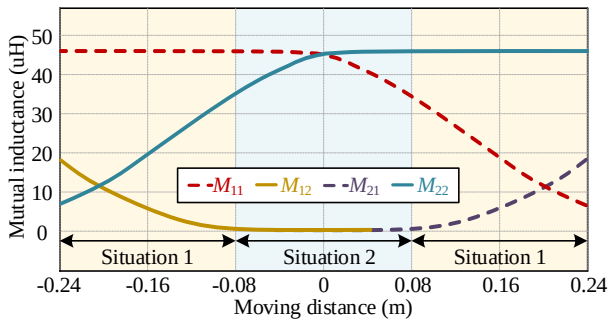

Fig. 13. Zoom-in trends of mutual inductances between track and receiver coils in the adjacent area of the track coils.

1) When the receiver is located in the middle range of the track coils, as indicated in Fig. 11(a) and marked as ① in Fig. 12, V_{s1} and V_{s2} are equal, and the receiver operates in Mode A. Both receiver coils are averagely picking power. The length of the track coils limits the area proportion of Mode A. The longer the track coils, the larger area of Mode A.

2) When there is a slight but nonnegligible difference between V_{s1} and V_{s2}, as shown in Fig. 11(b) and marked as ② in Fig. 12, the receiver will turn into Mode B. According to the analysis in Section III.B, since R_{s1} and R_{s2} are small, Mode B occupies much less area than other modes. Moreover, owing to negligible mutual inductances between the receiver coils and the next-segment track coils, the output voltage of the VD rectifier can still be the same as that in Mode A.

3) When the balance of the induced voltages of the receiver coils is broken, the receiver will turn into Mode C with only one receiver coil transferring power, as shown in Fig. 11(c) and marked as ③ in Fig. 12. Although the mutual inductance between receiver coil #2 and track coil #2 M_{22} increases sharply, the total induced voltage of receiver coil #2 V_{ob} is still lower than V_{ao}. Thus, only receiver coil #1 picks power from track coil #1, and the CV output can be maintained.

4) As shown in Fig. 11(d), when the receiver is aligned above the adjacent area of the track coils, the induced voltages of the receiver coils will briefly be balanced, and the receiver will operate in Mode B again. However, compared with other situations, the corresponding area of this situation is narrow, and the dynamic process is also short in the moving process.

D. Output Characteristic When the Receiver Moves above the Adjacent Area of the Track Coils

Based on the characteristic of the proposed DWPT system, when the receiver moves above the adjacent part of track coils, two main operation situations are analyzed as follows.

In the first situation, for example, receiver coil #2 is located on the adjacent part of the track coils, and receiver coil #1 is strongly coupled with track coil #1, as shown in Fig. 11(c). Here, the trends of the mutual inductances between the track coils and receiver coils are plotted in the yellow areas of Fig. 13. Although the induced voltage v_{s2} is the sum of the induced voltage from two track coils, M_{11} is still much higher than the sum of M_{12} and M_{22}. Thus, even if there is voltage oscillation on v_{s2}, only receiver coil #1 can transfer power individually, and the voltage oscillation will not result in power oscillation.

In the second situation, the receiver is nearly aligned with the adjacent part of the track coils, as shown in Fig. 11(d). The induced voltage of a single receiver coil is designed to mainly couple with only one track coil. The corresponding trends of the corresponding trends of the mutual inductances are plotted in the blue area of Fig. 13. Since M_{12} and M_{21} can be regarded as zero, there is no voltage oscillation in both v_{s1} and v_{s2}, even though the current frequencies in track coils are different. Thus, when M_{11}>M_{22}, i.e., V_{s1}>V_{s2}, only receiver coil #1 will transfer power, and power oscillation can also be avoided. Correspondingly, when M_{11}<M_{22}, only receiving coil #2 will output power to the load.

In particular, when the receiver is well-aligned above the adjacent area of the track coils, which means M_{11}=M_{22}, the induced voltages of the receiver coils will briefly turn completely balanced, and the power oscillation may occur again.

This article has been accepted for publication in IEEE Transactions on Industrial Electronics. This is the author's version which has not been fully edited and content may change prior to final publication. Citation information: DOI 10.1109/TIE.2022.3217592

Luckily, the corresponding area that may occur power oscillation is extremely narrow, and no fluctuation phenomena will be observed in the dynamic test, as introduced in Section III. E.

E. Dynamic Performance of the Proposed System

To verify the dynamic performance of the proposed DWPT system, the simulated mutual inductance results of the designed magnetic coupler for the proposed DWPT system are also inputted to MATLAB/Simulink. Here, all the circuit parameters except the parameters of the receiver coils are the same in TABLE II. The self-inductances L_{s1} and L_{s2} are about 188 uH, and the ESRs R_{s1} and R_{s2} are about 0.21 Ω. Similarly, R_L and system output power are set as 60.5 Ω and 800 W. Fig. 14 shows the dynamic simulation waveforms of the proposed DWPT system. It is obvious that the proposed system can provide a stable output voltage V_o by flexibly switching the operation mode of the rectifier without any extra controllers. Even if the frequency of i_{p2} is increased to (1+2‰)·f and (1+5‰)·f, the output characteristic of the proposed system is well maintained, and the fluctuation V_o is limited to 1.42% (@(1+2‰)·f) and 1.56% (@(1+5‰)·f) of the rated value.

In conclusion, in the proposed system, the constant output voltage can always be achieved when the receiver moves along the track. Even if the current frequencies of the adjacent track coils are different, since only the receiver coil with higher induced voltage can transfer power from only one track coil, the power oscillation can be well avoided.

F. Misalignment Effect on the Proposed System

Actually, the vehicles employing DWPT systems are always track-constrained or program-controlled to form a relatively fixed route with little misalignment. Even if the lateral misalignment occurs, both the receiver coils will synchronously misalign to the left or right with the vehicle.

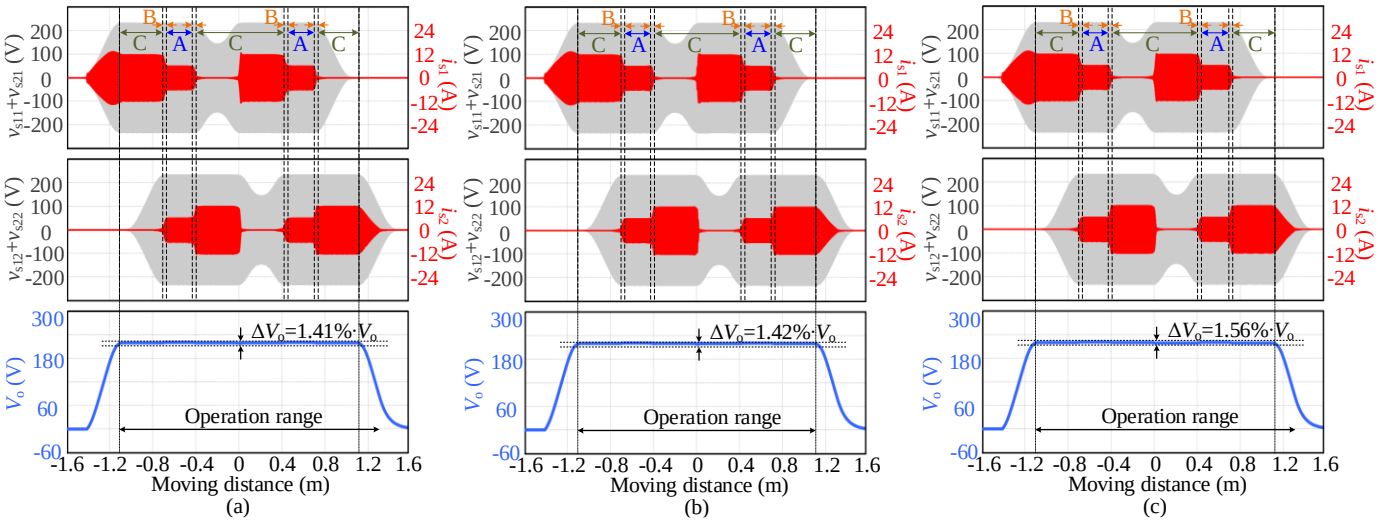

Fig. 14. The dynamic waveforms of the induced voltages and currents of receiver coils, system output voltage of the proposed dual-receiver system when the current frequency of i_{p1} is f, and the current frequency of i_{p2} is (a) f, (b) (1+2‰)·f, and (c) (1+5‰)·f.

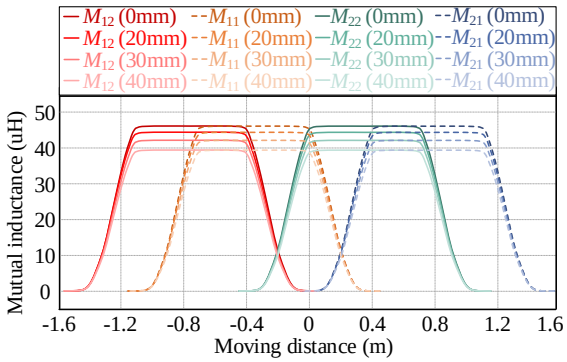

Fig. 15. Mutual inductances between track coils and receiver coils with different misalignment conditions.

Therefore, since the misalignment distances of both the receiver coils are almost the same when the receiver moves along the track coils, the proposed three operation modes are still valid. To verify the system output characteristic under misalignment conditions, the mutual inductances trends between the receiver coils and track coils with different misalignment distances are plotted in Fig. 15. Although the mutual inductances between the receiver and track coils will decrease when misalignment happens, the constant output characteristic can be still maintained. When the misalignment distance reaches 40 mm (10% of the receiver coil width), the system coupling can be maintained at ~85% of the rated values, which is an acceptable drop under the lateral misalignment condition.

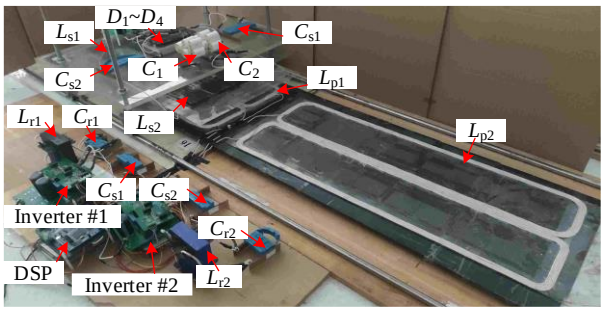

Fig. 16. The experimental setup.

IV. Experimental Verification

In order to validate the proposed circuit topology and the magnetic coupler, a 220 V-800 W experimental setup is built, as shown in Fig. 16. The track coils and the receiver coils are

built within the dimensions listed in TABLE I. Digital signal processors (DSPs) are used for driving the inverters.

A. Experimental Waveforms

1) FB rectifier mode

When both the receiver coils are above the middle range of the same track coil, the induced voltages V_{s1} and V_{s2} are balanced. Thus, the receiver operates in FB rectifier mode introduced in Section III.B, and its waveforms are shown in Fig. 17(a). Here, the currents in receiver coils I_{s1} and I_{s2} are also balanced. When R_L is set as 60.5 Ω, and the output power P_{out} is set as ~800 W, the system efficiency is ~93.6% to ~93.9%.

2) VD rectifier with Dual Coil Receiving Power Mode

When the receiver operates in Mode B, there is a tiny difference between V_{s1} and V_{s2}. Since v_{s1} and v_{s2} have the same frequency and are in phase, both the receiver coils are transferring power synchronously with an apparent difference in the RMS value of coil currents. The key waveforms are shown in Fig. 17(b). When P_{out} is ~800 W, the system efficiency is about ~93.0% to ~93.5%, which depends on the difference between the induced voltages of the receiver coils.

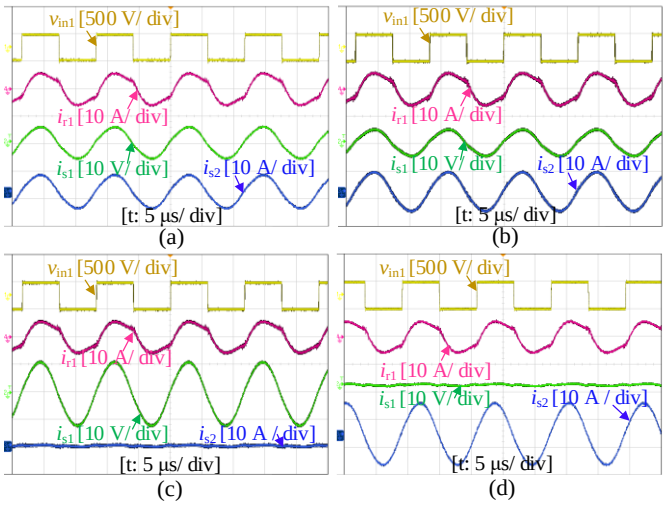

Fig. 17. Experimental waveforms of v_{in1}, i_{r1}, i_{s1}, and i_{s2} when the receiver operates in Mode (a) A, (b) B, (c) C with $V_{ao}>V_{ob}$, and (d) $V_{ao}<V_{ob}$.

3) VD rectifier with Single Coil Receiving Power Mode

When V_{ao} and V_{ob} significantly differ, the rectifier operates in the VD rectifier with single coil receiving power mode. When $V_{s1}>V_{s2}$, the key waveforms are shown in Fig. 17(c). Only receiver coil #1 transfers power, and I_{s2} is kept at zero. Compared with the corresponding waveforms in Fig. 17(a), I_{s1} is doubled to offer equal system output power. When $V_{s1}<V_{s2}$, the corresponding waveforms are shown in Fig. 17(d). Similarly, I_{s1} is kept at zero, and only receiver coil #2 transfers power. Within this operation mode, when P_{out} is ~800 W, the experimental efficiency of the DWPT system will vary from ~90.7% to ~93.0%, which is affected not only by the characteristic of this operation mode but also by the fabrication tolerance of the hand-made coils.

B. System Output Voltage and Efficiency

The trends of the system output voltage and the system efficiency against the moving distance are plotted in Fig. 18. With the proposed DWPT system, When the frequencies in the two adjacent track coils are the same, the fluctuation of the system output voltage V_o is limited to ~3.1% (~-1.5% to ~+1.6%), which is mainly caused by the fabrication tolerance of the hand-made coils. Meanwhile, when the current frequency in DD track coil #2 is set as (1+2‰)·f and (1+5‰)·f, the fluctuation of the voltage V_o is about ~3.6% (~-1.9% to ~+1.7%) and ~3.4% (~-1.7% to ~+1.7%). Even if the receiver moves above the adjacent part of the track coils, the system output voltage is still maintained at a constant value. Moreover, the system overall efficiency can be maintained from ~90.7% to ~93.8%, even though the track coil currents are different in frequency.

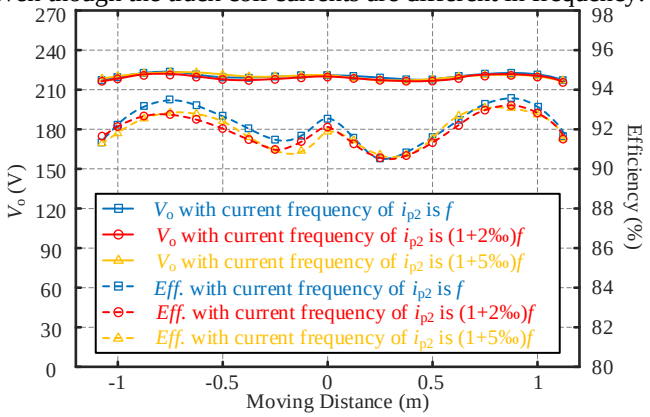

Fig. 18. V_o and the system efficiency against the moving distance.

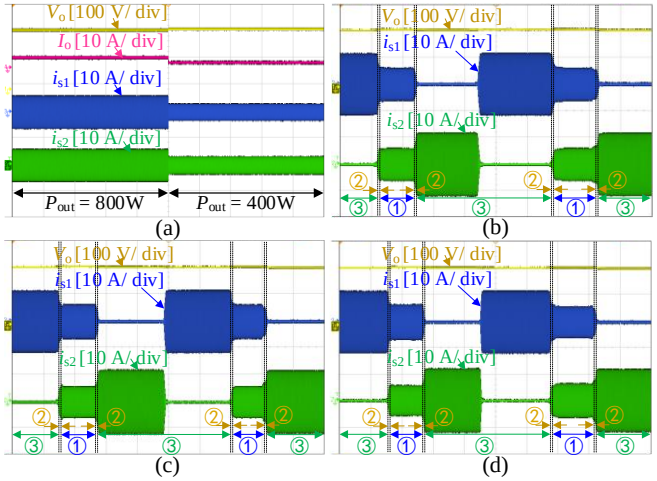

Fig. 19. (a)Waveforms of V_o, I_o, i_{s1}, i_{s2} when P_{out} changed from 800W to 400W, and waveforms of V_o, i_{s1}, i_{s2} when the receiver is moving along the track with the frequency of i_{p2} is (b) f, (c) (1+2‰)·f, and (d) (1+5‰)·f.

C. Dynamic Experiment

To verify the dynamic performance of the proposed DWPT system, the dynamic waveforms are recorded and provided. When the RMS values of V_{s1} and V_{s2} are equal, i.e., the system operates in Mode A, both receiver coils transfer power with the same coil currents. Here, when the system output power P_{out} changes from 800 W to 400 W, due to the CV characteristic of the LCC-S compensation, the system output voltage V_o is well maintained, and the currents in both receiver coils are halved simultaneously, as shown in Fig. 19(a). Moreover, when the receiver moves along the track and P_{out} is set to 800W, V_o can still be kept at a constant value with no apparent voltage fluctuation or any current oscillation, as shown in Fig. 19(b). The operation range of Mode A, B, and C are marked as ①, ②, and ③. Similarly, even if the frequency of i_{p2} is set as (1+2‰)·f and (1+5‰)·f, as shown in Fig. 19(c) and (d), there is still no oscillation on V_o when the receiver is moving above

the adjacent part of the track coils, which proves the good dynamic performance of the proposed system.

D. Comparison with the Other Power Fluctuation Suppression Methods for DWPT Systems

Several previous methods have been aimed at power fluctuation suppression for DWPT systems. In [12] and [15], the coupler size optimization method is proposed to provide a smooth output for the DWPT system. However, due to the strong cross-coupling between the transmit coils, assistant coils should be arranged to eliminate the effect caused by cross-coupling, resulting in extra cost and complexity. To solve this issue, the bipolar coil [28] and adjacent unipolar-DD coil [11] are introduced to the transmitter in the DWPT system. By simply adjusting the dimensions of the transmitters and receivers, the power fluctuation in the moving process can be further suppressed. Moreover, based on misalignment tolerance improvement methods for statics wireless power transfer systems, an integrated magnetic coupler is proposed to improve the dynamic output characteristic of the DWPT system [29], which also achieves good output stability. In addition to the single receiver coil system, the multi-receiver structure with the corresponding circuit topology is introduced in [25]. With the n-type transmitter coils, the system fluctuation can be apparently reduced. Although these methods above can effectively improve the system output stability, the power oscillation caused by the current frequency difference between adjacent track coils is still disregarded and unavoidable.

Compared with these methods above, this paper's main contribution is eliminating the power oscillation phenomena when the receiver moves above the adjacent part of the track coils by adopting dual-receiver coils and the VD rectifier. Even though there is a tiny current frequency difference between the adjacent track coils, the system output voltage can still be maintained at a constant value since only the receiver coil with higher induced voltage can transmit power from only one track coil individually. In addition, with the well-designed coupler in the experimental setup, the proposed system also has advantages in output power fluctuation suppression.

TABLE III SUMMARY AND COMPARISON WITH OTHER POWER FLUCTUATION SUPPRESSION METHODS FOR DWPT SYSTEM

Ref.	Coupler structure	Air gap	Dynamic output voltage(V) / power (P) fluctuation	Output power	Maximum efficiency	Power oscillation caused by the frequency difference
[12]	Tx: DDQ, Rx: Q	100 mm	V: within ±2.5%	~259W	90%	Not considered
[15]	Tx: DDQ, Rx: Q	150 mm	P: ±7.5%	~1.4kW	89.78%	Not considered
[28]	Tx: Q, Rx: Q	50 mm	V: within ±2%	~167W	87%	Not considered
[11]	Tx: DD&Q, Rx: DDQ	100 mm	V: within ±2%	~384W	90.374%	Not considered
[29]	Tx: Q&Q, Rx: Q&Q	150 mm	P: within ±4%	~4.5kW	91.6%	Not considered
[25]	Tx: n-type, Rx: DD (4-phase)	170mm	V: within ±7.3%	~10kW		Not considered
This paper	Tx: DD, Rx: DD	80 mm	P: -2.6% to +3.2% V: -1.5% to +1.6%	~800W	93.8%	Eliminating

V. CONCLUSION

This work proposes an output power fluctuation suppression method based on dual-receiver coils and a VD rectifier for the DWPT system. With the designed magnetic coupler, the proposed DWPT system can provide a CV characteristic when the receiver moves along the track and avoid power oscillation caused by coupling fall area and the currents in the adjacent track coils that are desynchronized. According to the circuit modelling and mathematical analysis, the operation modes of the proposed receiver topology are divided, and the specific characteristics in each mode, including the transfer power division of the dual receiver coils, are analyzed. The experimental results of the built 2.2 m-DWPT prototype show that the proposed DWPT system can limit the fluctuation of the system output voltage at a low level. Even if there is a tiny frequency difference between the adjacent track coils, since only one of the receiver coils can transfer power with doubled output voltage while the other one is clamped with no output power, the voltage fluctuation is generally less than 3.6%. Meanwhile, the system overall efficiency in the whole moving process can achieve >90.7% with an 8cm air gap.

REFERENCES

[1] S. Choi, B. Gu, S. Jeong, and C. Rim, "Advances in wireless power transfer systems for roadway-powered electric vehicles," *IEEE Jour. of Emerg. Sel. Top. Power Electron.*, vol. 3, pp. 18-36, Mar. 2015.

[2] G. Covic and J. Boys, "Modern trends in inductive power transfer for transportation applications," *IEEE J. Emerg. Sel. Top. Power Electron.*, vol. 1, no. 1, pp. 28–41, Mar. 2013.

[3] C. Mi, G. Buja, S. Choi, and C. Rim, "Modern advances in wireless power transfer systems for roadway powered electric vehicles," *IEEE Trans. Ind. Electron.*, vol. 63, no. 10, pp. 6533–6545, Oct. 2016.

[4] S. Jeong, Y. Jang, and D. Kum, "Economic analysis of the dynamic charging electric vehicle," *IEEE Trans. Power Electron.*, vol. 30, No. 11, pp. 6368-6377, Nov. 2015.

[5] W. Liu, K. Chau, C. Lee, C. Jiang, and W. Han, "A switched-capacitorless energy-encrypted transmitter for roadway-charging electric vehicles," *IEEE Trans. Magn.*, vol. 54, no. 11, pp. 1-6, Nov. 2018.

[6] M. Kissin, J. Boys, and G. Covic, "Interphase mutual inductance in polyphase inductive power transfer systems," *IEEE Trans. Ind. Electron.*, vol. 56, no. 7, pp. 2393–2400, Jul. 2009.

[7] J. Huh, S. Lee, W. Lee, G. Cho, and C. Rim, "Narrow-width inductive power transfer system for on-line electrical vehicles," *IEEE Trans. Power Electron.*, vol. 26, no. 12, pp. 3666–3679, Dec. 2011.

[8] S. Lee, J. Huh, C. Park, N. Choi, G. Cho, and C. Rim, "On-line electric vehicle using inductive power transfer system," in *Proc. IEEE Energy Convers. Congr. Exposit.*, Sep. 2010, pp. 1598–1601.

[9] S. Ahn and J. Kim, "Magnetic field design for high efficient and low EMF wireless power transfer in on-line electric vehicle," in *Proc. 5th Eur. Conf. Antennas Propag.*, Apr. 2011, pp. 3979–3982.

[10] E. Lee, M. Kim, S. Kang, and S. Han, "Segmented IPT coil design for continuous multiple charging of an electrified monorail system," *IEEE Trans. Power Electron.*, Early Access.

[11] Y. Li, J. Hu, T. Lin, X. Li, F. Chen, Z. He, and R. Mai, "A new coil structure and its optimization design with constant output voltage and constant output current for electric vehicle dynamic wireless charging," *IEEE Trans. Ind. Inform.*, vol. 15, no. 9, pp. 5244-5256, Sept. 2019.

[12] X. Li, J. Hu, H. Wang, X. Dai, and Y. Sun, "A new coupling structure and position detection method for segmented control dynamic wireless power transfer systems," *IEEE Trans. Power Electron.*, vol. 35, no. 7, pp. 6741-6745, Jul. 2020.

[13] S. Choi, J. Huh, W. Lee, S. Lee, and C. Rim, "New cross-segmented power supply rails for roadway-powered electric vehicles," *IEEE Trans. Power Electronics*, vol. 28, no. 12, pp. 5832-5841, Dec. 2013.

[14] J. Miller, P. Jones, J. Li, and O. Onar, "ORNL experience and challenges facing dynamic wireless power charging of EV's," *IEEE Circuits Syst. Mag*., vol. 15, no. 2, pp. 40-53, May 2015.
[15] F. Lu, H. Zhang, H. Hofmann, and C. Mi, "A dynamic charging system with reduced output power pulsation for electric vehicles," *IEEE Trans. Ind. Electron.*, vol. 63, no. 10, pp. 6580-6590, Oct. 2016.
[16] S. Li, L. Wang, Y. Guo, and Z. Liu, "Flexible energy-transfer control of dynamic wireless power transfer system based on estimation of load and mutual inductance," *IEEE Trans. Ind. Appl.*, vol. 58, no. 1, pp. 1157-1167, Jan.-Feb. 2022.
[17] S. Liu, R. Mai, L. Zhou, Y. Li, J. Hu, Z. He, Z. Yan, and S. Wang, "Dynamic improvement of inductive power transfer systems with maximum energy efficiency tracking using model predictive control: analysis and experimental verification," *IEEE Trans. Power Electron.*, vol. 35, no. 12, pp. 3794-3806, Dec. 2020.
[18] Y. Yang, W. Zhong, S. Kiratipongvoot, S. Tan, and S. Hui, "Dynamic improvement of series–series compensated wireless power transfer systems using discrete sliding mode control," *IEEE Trans. Power Electron.*, vol. 33, no. 7, pp. 6351-6360, Jul. 2018.
[19] Z. Huang, S. Wong, and C. Tse, "Control Design for Optimizing Efficiency in Inductive Power Transfer Systems," *IEEE Trans. Power Electron.*, vol. 33, no. 5, pp. 4523-4534, May 2018.
[20] X. Dai, J. Jiang, and J. Wu, "Charging area determining and power enhancement method for multiexcitation unit configuration of wirelessly dynamic charging EV system," *IEEE Trans. Ind. Electron.*, vol. 66, no. 5, pp. 4086–4096, May. 2019.
[21] C. Cai, M. Saeedifard, J. Wang, P. Zhang, J. Zhao, and Y. Hong, "A cost-effective segmented dynamic wireless charging system with stable efficiency and output power," *IEEE Trans. Power Electron.*, vol. 37, no. 7, pp. 8682-8700, Jul. 2022.
[22] F. Zhao, J. Jiang, S. Cui, X. Zhou, C. Zhu, and C. Chan, "Research on bipolar nonsalient pole transmitter for high-power EV dynamic wireless power transfer system," *IEEE Trans. Power Electron.*, vol. 37, no. 2, pp. 2404-2412, Feb. 2022.
[23] L. Jiang, L. Shi, M. Fan, F. Zhang, and Y. Li, "Segment control scheme of inductive power transfer system for rail transit," *IEEE Trans. Ind. Appl*., vol. 54, no. 4, pp. 3271-3280, July-Aug. 2018.
[24] H. Li, Y. Liu, K. Zhou, Z. He, W. Li, and R Mai, "Uniform power IPT system with three-phase transmitter and bipolar receiver for dynamic charging," *IEEE Trans. Power Electron.*, vol. 34, no. 3, pp. 2013-2017, Mar. 2019.
[25] S. Cui, Z. Wang, S. Han, C. Zhu, and C. Chan, "Analysis and design of multiphase receiver with reduction of output fluctuation for EV dynamic wireless charging system," *IEEE Trans. Power Electron.*, vol. 34, No. 5, pp. 4112-4124, May. 2019.
[26] J. Zhao, T. Cai, S. Duan, H. Feng, C. Chen, and X. Zhang, "A general design method of primary compensation network for dynamic WPT system maintaining stable transmission power," *IEEE Trans. Power Electron.*, vol. 31, no. 12, pp. 8343-8358, Dec. 2016.
[27] Y. Geng, Z. Yang, and F. Lin, "Design and control for catenary charged light rail vehicle based on wireless power transfer and hybrid energy storage system," *IEEE Trans. Power Electron.*, vol. 35, no. 8, pp. 7894-7903, Aug. 2020.
[28] C. Cai, M. Saeedifard, J. Wang, P. Zhang, J. Zhao, and Y. Hong, "A cost-effective segmented dynamic wireless charging system with stable efficiency and output power," *IEEE Trans. Power Electron.*, vol. 37, no. 7, pp. 8682-8700, Jul. 2022.
[29] K. Shi, C. Tang, Z. Wang, X. Li, Y. Zhou, and Y. Fei, "A magnetic integrated method suppressing power fluctuation for EV dynamic wireless charging system," *IEEE Trans. Power Electron.*, vol. 37, no. 6, pp. 7493-7503, Jun. 2022.

Shunpan Liu (S'19) received the B.S. degree in electrical engineering and automation from the School of Electrical Engineering, Southwest Jiaotong University, Chengdu, China, in 2018, where he is currently working toward the Ph.D. degree. His main research interest focuses on wireless power transfer, especially on control method and circuit topology of dynamic inductive power transfer system.

Yong Li (M'20-SM'21) received the B.Sc. and Ph.D. degrees from the School of Electrical Engineering, Southwest Jiaotong University, Chengdu, China, in 2013 and 2017, respectively. From 2017 to 2018, he was a Research Associate with the Department of Electrical Engineering, The Hong Kong Polytechnic University, and subsequently, he was a Post-Doctoral Fellow. He is currently an Associate Professor with Southwest Jiaotong University. His main research interests include wireless power transfer and microgrids.

Yihao Wu (S'21) received the B.Eng. degree from the Southwest Jiaotong University, Chengdu, China, the B.Eng. (first-class Hons.) degree from the University of Leeds, Leeds, U.K. both in 2020, and the M.Sc. (distinction) degree from Imperial College London, London, U.K. in 2021. He is currently working toward the Ph.D. degree with the Department of Electrical and Computer Engineering, the University of Texas at Austin, Austin, TX, USA. His main research interest are wireless power transfer and DC-DC converters.

Lingyun Zhou (S'19) received the B.S. degree in electrical engineering and automation from the School of Electrical Engineering, Southwest Jiaotong University, Chengdu, China, in 2018, where she is currently working toward the Ph.D. degree. Her main research interest focuses on wireless power transfer, especially on efficiency improvement for low power devices.

Xing Zhao (Member, IEEE) received the B.Eng. degree from Nanjing University of Aeronautics and Astronautics, Nanjing, China, in 2014, and the Ph.D. degree from The Hong Kong Polytechnic University, Hong Kong SAR, in 2020, both in Electrical Engineering. He is currently a Lecturer in the School of Physics, Engineering and Technology with University of York, UK. His research interests include advanced electrical machines and power electronics for electric vehicles and renewable energy systems.

Ruikun Mai (M'14) received the B.Sc. and Ph.D. degrees in electrical engineering from the School of Electrical Engineering, Southwest Jiaotong University, Chengdu, China, in 2004 and 2010, respectively. He is currently a Professor with the School of Electrical Engineering, Southwest Jiaotong University, Chengdu, China. His research interests include wireless power transfer and its application in railway systems, power system stability and control.

Zhengyou He (M'10-SM'13) received the B.S. and M.S. degrees from Chongqing University, Chongqing, China, in 1992 and 1995, respectively, and the Ph.D. degree from Southwest Jiaotong University, Chengdu, in 2001. Since 2002, he has been a Professor with the School of Electrical Engineering, Southwest Jiaotong University. He was a Visiting Scholar with Cornell University, NY, USA, from 2008 to 2009. His research interests are in the area of signal processing and information theory and its application in electrical power systems, and the application of wavelet transforms in power systems